

Alkyl side chain effects of optically active polyfluorenes on their chiroptical absorption and emission properties

Hong-Zhi Tang^{a,1}, Michiya Fujiki^{a,b,*}, Masao Motonaga^a

^aCREST-JST (Japan Science and Technology Corporation), 4-1-8 Hon-cho, Kawaguchi, Saitama 332-0012, Japan

^bGraduate School of Materials Science, Nara Institute of Science and Technology (NAIST), 8916-5 Takayama, Ikoma, Nara 630-0101, Japan

Received 1 April 2002; received in revised form 13 August 2002; accepted 20 August 2002

Abstract

We prepared three optically active polyfluorenes (PFs), poly[2,7-(9,9-bis[(*S*)-2-methyloctyl]]fluorene] (**S1**) and poly[2,7-(9,9-bis[(*S*)-and/or (*R*)-3,7-dimethyloctyl]]fluorene] (**S2** and/or **R2**) and an optically inactive poly[2,7-(9,9-di-*n*-decyl)fluorene] (**3**) in order to investigate the alkyl side-chain effects on their (chir)optical properties in both solution and solid states. PF **S1** showed more intense circular dichroism (CD) signals in THF solution at higher and lower temperatures due to a stiffer backbone structure. Although the CD and UV–visible spectra suggested that similar thermally driven order–disorder conformational transitions occurred for all of these PFs, the highly ordered conformations formed upon cooling showed less planar structures with the stereocenters closer to the PF backbones, whose planarity decreased in the order of **3**, **S2/R2**, and **S1**. In the pristine spin-coated films on quartz, with the stereocenters closer to the PF backbones, the corresponding PFs showed more intense bisignate CD signals and blueshifts in the emission peaks. © 2002 Published by Elsevier Science Ltd.

Keywords: Polyfluorene; Chiroptical properties; Side-chain effects

1. Introduction

Polyfluorene (PF), a class of π -conjugated polymers, has recently attracted increasing interest, due to its bluish photo- and/or electro-luminescence with high quantum yield, high hole-transporting property, and excellent thermal, chemical, and photochemical stabilities [1–32].

PF bearing linear alkyl side chains [3–17] such as *n*-hexyl and *n*-octyl, particularly, attracted much research interest, due to its thermotropic liquid crystallinity and large dichroic ratios in both absorption and emission in an aligned thin film. PF bearing linear ether side chains such as 3,6-dioxaheptyl, was first synthesized by Pei and Yang [18]. The ether side chains function to solvate ions and promote ion transport as required for high-performance solid-state light-emitting electrochemical cells (LECs). In addition, PF having branched side chains such as 2-ethylhexyl [19–23], being suggested to take helical structures in a thermally

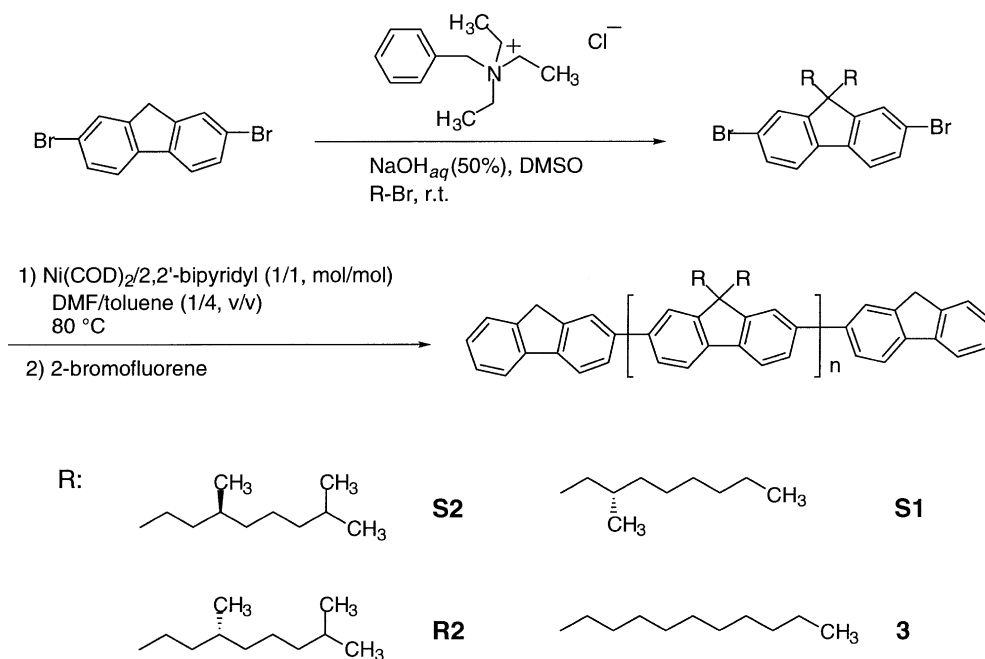
treated solid [19], exhibits larger dichroic ratios up to 16 in an aligned thin film on a rubbed polyimide substrate. Moreover, PF featuring bulky dendritic side chains was demonstrated to emit an almost pure blue color without featureless excimer emission with a green color even in an annealed thin film [24–28]. We recently designed and synthesized the first unsymmetrically substituted PF bearing a bulky poly(benzyl ether) dendron and less bulky 3,6-dioxaoctyl side chains, which strongly suppresses the greenish excimer emission in an annealed thin film compared to the symmetrically 9,9-di-dendron-substituted PF [28].

On the other hand, Oda, Neher, and coworkers synthesized the first optically active PF bearing highly enantiopure alkyl side chains, poly[2,7-(9,9-bis[(*S*)-3,7-dimethyloctyl]]fluorene] (**S2**), showing intense circular dichroism (CD) and especially, intense circularly polarized electroluminescence (CPEL) in an annealed thin film [29, 30]. However, no detailed information on the solution-state chiroptical properties was provided, because **S2** featuring stereocenters at the γ -position showed no optical activity in good solvents at room temperature. Recently, we reported that PF featuring stereocenters at the β -position in the

* Corresponding author. Tel.: +81-743-72-6040.

E-mail addresses: fujikim@ms.aist-nara.ac.jp (M. Fujiki), tanghz@u.washington.edu (H.Z. Tang).

¹ Present address: Department of Materials Science and Engineering, University of Washington, Seattle, WA 98195-2120, USA.



Scheme 1.

highly enantiopure alkyl side chains, poly[2,7-(9,9-bis[(*S*)-2-methyloctyl]]fluorene] (**S1**), showed optical activity in good solvents even at high temperatures [31,32]. Particularly, PF **S1**, in a molecularly dispersed solution-state in a good solvent, exhibits a thermally driven order–disorder conformationally transitional phenomenon as shown in Fig. 2 [32].

The stereocenters in the side chains of a polymer play an important role in determining the polymer conformation and properties. Fujiki and coworkers have given much attention to a systematic study of such effects on the conformations and the chiroptical properties of polysilanes [33–35]. This is because that such a systematic study is extremely helpful to obtain a comprehensive understanding of a polymer for guiding the design and synthesis of a new polymer aimed at unique novel functionality.

Although there have been many reports on the syntheses, structures, and properties of PFs [1–32], knowledge of the relationship between the (chir)optical properties and the side-chain effects of optically active PFs may be lacking. In the present study, to obtain the (chir)optical properties–side chains relationship, we prepared three optically active PFs bearing alkyl side chains including (*S*)-2-methyloctyl, (*S*)/(*R*)-3,7-dimethyloctyl, featuring stereocenters at the β - and/or γ -positions, together with an optically inactive PF having linear *n*-decyl side chains (Scheme 1). Here we report and discuss the alkyl side-chain effects on the chiral/achiral optical properties of the PFs in both solution and thin film states by means of CD/UV–visible and circularly polarized photoluminescence (CPL)/photoluminescence (PL) techniques together with viscometric studies.

2. Experimental

2.1. Materials

All commercial chemicals were used without further purification. Spectroscopic grade THF (Kanto) was used for preparing the polymer solutions for measurements. (*S*)-2-Methyloctyl bromide was synthesized at the Chemical Soft Co. (Kyoto, Japan) by bromination of (*S*)-2-methyl-1-octanol (Japan Energy, Tokyo, Japan, $[\alpha]_D^{25} = -9.6^\circ$ (neat), $\geq 89\%$ ee, noted in *Chiral Reagents* 1600, p. 213). (*R*)- and (*S*)-3,7-Dimethyloctyl bromide [(*R*)-form: $[\alpha]_D^{24} = -5.96^\circ$ (neat), 96.0% ee; (*S*)-form: $[\alpha]_D^{24} = +6.05^\circ$ (neat), 96.2% ee] were also obtained from the Chemical Soft Co.

2.2. Instrumentation

¹H (300.0 MHz) and ¹³C (75.4 MHz) NMR spectra were recorded in CDCl₃ at room temperature with a Varian Unity 300 NMR spectrometer using tetramethylsilane as an internal standard. Elemental analyses were performed at the Toray Research Center (TRC, Shiga, Japan) using a Vario elemental analysis apparatus. Optical rotation at the Na–D line was measured with a JASCO DIP-370 polarimeter using a quartz cell with a path length of 1.0 cm at room temperature. Molecular weights were evaluated by size exclusion chromatography (SEC) on a Shodex KF806 M column (eluent THF, +30 °C) using a Shimadzu liquid chromatography instrument equipped with a photodiode array detector based on the calibration with polystyrene standards. The intrinsic viscosity–molecular weight relationship in THF at +30 °C was performed using an in-line configuration of a viscometer (Viscotek T60A)

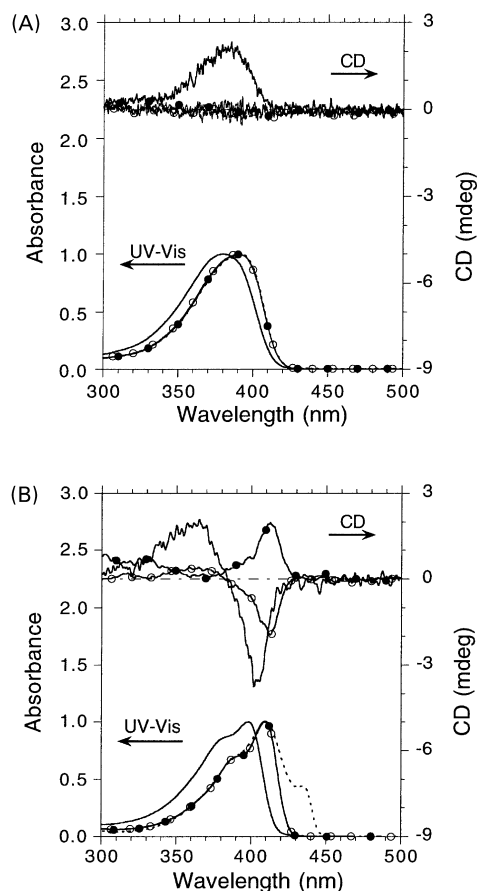


Fig. 1. CD and UV-visible spectra of the PFs (thick solid line for **S1**; thin solid line with open circles for **S2**; thin solid line with filled circles for **R2**; dotted line for **3**) in THF solution at +50 °C (A) and -80 °C (B). The UV-visible spectrum of **3** was recorded at -60 °C. Run 1 sample of **S1** was used.

and the SEC (Shimadzu) instrument. CD and UV-visible spectra were recorded simultaneously on a JASCO J-725 spectropolarimeter equipped with a Peltier control for temperatures from +50 to -10 °C (cell path: 1.0 cm) and a liquid nitrogen-controlled quartz cell with a path length of 0.5 cm in a cryostat, ranging from room temperature to -80 °C. The solution concentrations of the PFs in THF were 3.0×10^{-5} M of the fluorene (FL)-repeat-unit. The linear dichroism (LD) spectra in absorption were recorded on a JASCO J-820 spectropolarimeter with an LD attachment at room temperature at International Christian University (ICU, Mitaka, Tokyo). Non-polarized PL spectra in thin films on quartz substrates were collected in 45/45° angle geometry to minimize the self-absorption effects using a Hitachi 850 spectrofluorometer, or together with CPL spectra were recorded simultaneously on a JASCO CPL-200 spectrophotopolarimeter with an in-line configuration to allow for the determination of the photoluminescence dissymmetry factors under artifact-free conditions [36,37].

2.3. Syntheses

The synthetic procedure is outlined in Scheme 1. Using the phase transfer catalyst, triethylbenzyl ammonium chloride (Kanto), the monomers were synthesized from 2,7-dibromofluorene (Aldrich) and the corresponding alkyl bromide in high yields of ~90% [28,31,32]. Polymerization was carried out using a zero-valent nickel reagent, bis(1,5-cyclooctadiene)nickel(0) (Ni(COD)₂) (Kanto), and the end-termination was accomplished using 2-bromofluorene (Acros) [17,28,31,32].

2,7-Dibromo-9,9-bis[(S)-2-methyloctyl]fluorene.

$[\alpha]_D^{24} = -1.5^\circ$ (neat). ¹³C NMR: δ (ppm) 14.10, 21.67, 22.66, 26.25, 28.84, 29.22, 31.73, 38.28, 47.98, 55.29, 121.06, 121.14, 127.20, 130.14, 139.16, 152.56. Calcd for C₃₁H₄₄Br₂: C, 64.59; H, 7.69. Found: C, 64.65; H, 7.60%.

2,7-Dibromo-9,9-bis[(S)-3,7-dimethyloctyl]fluorene.

$[\alpha]_D^{24} = +5.3^\circ$ (neat). ¹³C NMR: δ (ppm) 19.46, 22.58, 22.67, 24.53, 27.91, 30.28, 32.75, 36.49, 37.41, 39.14, 55.49, 121.11, 121.45, 126.07, 130.13, 139.12, 152.46. Calcd for C₃₃H₄₈Br₂: C, 65.56; H, 8.00. Found: C, 65.88; H, 8.11%.

2,7-Dibromo-9,9-bis[(R)-3,7-dimethyloctyl]fluorene.

$[\alpha]_D^{24} = -5.6^\circ$ (neat). ¹³C NMR: δ (ppm) 19.47, 22.59, 22.67, 24.55, 27.94, 30.35, 32.80, 36.55, 37.43, 39.19, 55.54, 121.10, 121.50, 126.16, 130.19, 139.17, 152.52. Calcd for C₃₃H₄₈Br₂: C, 65.56; H, 8.00. Found: C, 65.85; H, 8.10%.

2,7-Dibromo-9,9-di-n-decylfluorene. ¹³C NMR: δ (ppm) 14.11, 22.66, 23.62, 29.20, 29.27, 29.50, 29.52, 29.86, 31.86, 40.15, 55.69, 121.12, 121.46, 126.17, 130.14, 139.07, 152.56. Calcd for C₃₃H₄₈Br₂: C, 65.56; H, 8.00. Found: C, 65.98; H, 8.12%.

S1: $M_w = 56,600$, $M_n = 18,300$ (Run 1); $M_w = 195,000$, $M_n = 76,900$ (Run 2). ¹³C NMR: δ (ppm) 14.09, 22.02, 22.68, 26.63, 29.11, 29.40, 31.78, 38.87, 48.42, 55.06, 119.90, 122.68, 126.21, 140.21, 140.36, 151.55. Calcd for C₃₁H₄₄: C, 89.36; H, 10.64. Found: C, 88.74; H, 10.70%.

S2: $M_w = 179,000$, $M_n = 58,700$. ¹³C NMR: δ (ppm) 19.58, 22.60, 22.69, 24.75, 27.93, 30.83, 32.98, 36.76, 37.63, 39.28, 55.14, 119.96, 121.58, 126.22, 140.14, 140.64, 151.74. Calcd for C₃₃H₄₈: C, 89.12; H, 10.88. Found: C, 88.77; H, 10.89%.

R2: $M_w = 189,700$, $M_n = 81,300$. ¹³C NMR: δ (ppm) 19.56, 22.59, 22.68, 24.73, 27.91, 30.79, 32.96, 36.75, 37.58, 39.26, 55.11, 119.92, 121.55, 126.19, 140.13, 140.61, 151.70. Calcd for C₃₃H₄₈: C, 89.12; H, 10.88. Found: C, 88.90; H, 10.93%.

3: $M_w = 211,300$, $M_n = 88,100$. ¹³C NMR: δ (ppm) 14.12, 22.67, 23.95, 29.31, 29.57, 29.62, 30.09, 31.90, 40.38, 55.35, 119.97, 121.50, 126.16, 140.03, 140.49, 151.83. Calcd for C₃₃H₄₈: C, 89.12; H, 10.88. Found: C, 88.92; H, 10.93%.

Table 1
Characteristics of UV–visible and CD absorptions of PFs in THF at +50 and –80 °C

	+50 °C			–80 °C			
	λ_{\max} (nm)	ϵ^a	$\Delta\epsilon^a$	λ_{\max} (nm)	ϵ^a	Extremum (nm)	$\Delta\epsilon^a$
S1 ^b	380.0	3.35×10^4	+2.1	399.0	4.54×10^4	355.0 403.0	+2.4 –4.7
S2	390.0	4.22×10^4	– ^c	409.5	6.19×10^4	409.5	–3.4
R2	390.0	4.14×10^4	– ^c	409.5	6.18×10^4	409.5	+3.1
3	391.0	4.78×10^4	– ^c	409.5 ^d 434.8 ^{d,e}	4.94×10^{4d} $2.17 \times 10^{4d,e}$		

^a Unit: (FL-repeat-unit)^{–1} dm³ cm^{–1}.

^b Run 1 sample of **S1**.

^c Not detected.

^d Temperature: –60 °C.

^e The newly appeared UV–visible absorption peak.

3. Results and discussion

3.1. Solution-state properties

3.1.1. CD/UV–visible spectra

Fig. 1 compares the CD and UV–visible spectra of PFs in THF (good solvent) at higher (A) and lower (B) temperatures. Table 1 summarizes the characteristics of UV–visible and CD absorptions. At a higher temperature of +50 °C, the CD spectrum of **S1** exhibits a positive-sign CD signal ($\Delta\epsilon = 2.1$ (FL-repeat-unit)^{–1} dm³ cm^{–1}), matching the maximum of the corresponding UV–visible absorption ($\lambda_{\max} = 380.0$ nm, $\epsilon = 3.35 \times 10^4$ (FL-repeat-unit)^{–1} dm³ cm^{–1}) due to the π – π^* transitions of the PF backbones, indicating that **S1** may assume a certain chiral conformation, e.g. a helix, in THF at +50 °C. On the contrary, extremely weak CD signals were observed for both **S2** and **R2**, implying that they both take random conformations in THF at +50 °C. As summarized in Table 1, the UV–visible spectra of **S2** and **R2** exhibit redshifts of 10 nm ($\lambda_{\max} = 390.0$ nm) in the absorption peaks and increases in the absorption intensity ($\epsilon = 4.22 \times 10^4$ for **S2**; $\epsilon = 4.14 \times 10^4$ for **R2**), suggesting that both **S2** and **R2** have longer conjugation lengths with

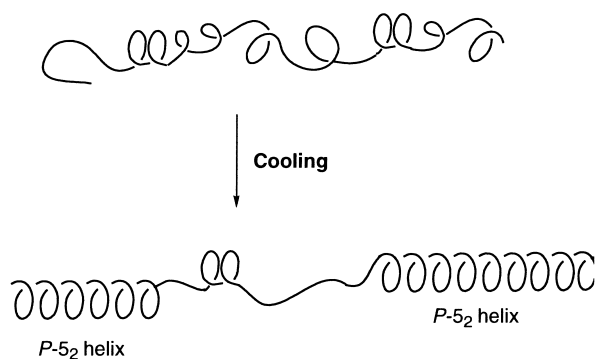


Fig. 2. Schematic models of the thermally driven conformational transition of **S1** from disordered local motifs with overall *M*-helicity in the stiff wormlike PF backbone at higher temperature to a highly ordered PF backbone motif of a *P*-5₂ helix along with other unclear local PF backbone motifs at lower temperature.

lower excitation energies in THF at +50 °C. Interestingly, the UV–visible spectrum of **3** in THF at +50 °C shows a more intense absorbance with ϵ of 4.78×10^4 , suggesting a much longer conjugation length, but an absorption maximum at 391.0 nm, almost identical to those of **R2** and **S2**.

Upon cooling from +50 to –80 °C, the broad UV–visible absorption band of **S1** at +50 °C changed gradually into a well-resolved band with a shoulder around 380 nm at –80 °C, exhibiting a significant redshift of 19 nm and a pronounced increase in the absorption intensity at the wavelength of the absorption peak ($\lambda_{\max} = 399.0$ nm, $\epsilon = 4.54 \times 10^4$); the single positive-sign CD band gradually changed into an apparent bisignate CD signal with a positive-sign CD band at a shorter wavelength of 355.0 nm ($\Delta\epsilon = +2.4$) and a negative-sign one at a longer wavelength of 403.0 nm ($\Delta\epsilon = -4.7$). As we recently reported [32], such CD and UV–visible spectral changes are related to a thermally driven order–disorder conformational transition. Fig. 2 shows the thermally driven conformational transition. At higher temperature of +50 °C, PF **S1**, in a molecularly dispersed solution-state in a good solvent of THF, took randomly twisted local PF backbone motifs in the wormlike PF backbone. Upon cooling, however, the molecularly isolated PF **S1** main chain adopted a highly ordered PF backbone motif, possibly a *P*-5₂ helix (The *P*-handedness is assumed here corresponding to the negative-sign CD band, and vice versa), together with other unclear local backbone motifs with the opposite screw sense at lower temperature. Additionally, it was demonstrated that PF main chains at the CD and UV–visible measured concentration of 3.0×10^{-5} M of the fluorene (FL)-repeat-unit are dispersed molecularly [32].

Similar changes in the UV–visible spectra as nearly the same redshifts of 19.5 nm in the absorption peaks and significant increases in the absorption intensity for **S2** and **R2** ($\lambda_{\max} = 409.5$ nm, $\epsilon = 6.19 \times 10^4$ for **S2**; $\epsilon = 6.18 \times 10^4$ for **R2**) were observed for **S2** and **R2** upon cooling from +50 to –80 °C. The very weak CD signals at +50 °C gradually changed into a negative-sign

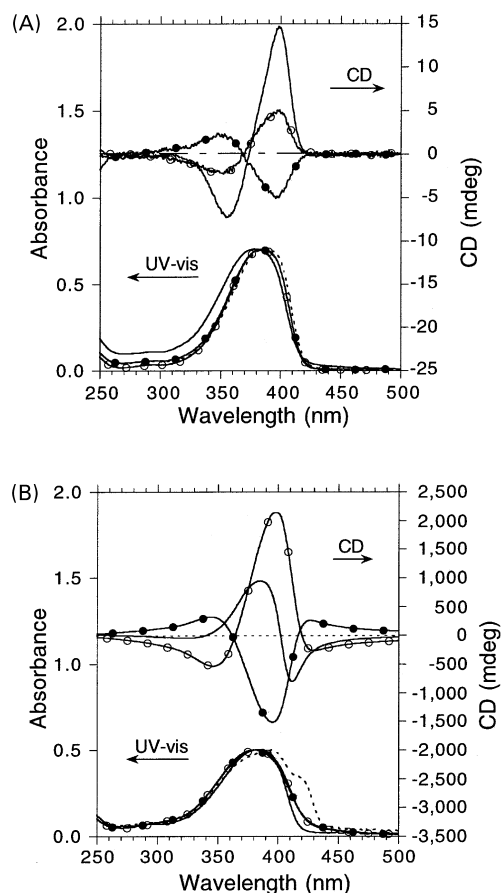


Fig. 3. CD and UV–visible spectra of the PFs (thick solid line for **S1**; thin solid line with open circles for **S2**; thin solid line with filled circles for **R2**; dotted line for **3**) in the spin-coated pristine films (A) and the annealed thin solid films (B). Run 2 sample of **S1** was used.

CD band ($\Delta\epsilon = -3.4$) at 409.5 nm with a shoulder around 392.0 nm for **S2**, and a positive-sign CD band ($\Delta\epsilon = +3.1$) at 409.5 nm with a shoulder around 392 nm for **R2**. This indicates that, upon cooling, similar thermally driven order–disorder conformational transitions occurred for **S2** and **R2**. The highly ordered motifs formed in the **S2** and **R2** backbones, however, may be more planar structures, which have longer conjugation lengths with lower excitation energies.

Upon cooling, however, a different changing mode in the UV–visible spectra of **3** was observed. The UV–visible spectrum of **3** in THF at $-60\text{ }^\circ\text{C}$ shows not only a redshift of 18.5 nm ($\lambda_{\text{max}} = 409.5\text{ nm}$, $\epsilon = 4.94 \times 10^4$) in the main absorption band but also, especially, a newly appearing well-resolved band at the longer wavelength of 434.8 nm ($\epsilon = 2.17 \times 10^4$), which is a characteristic for PF bearing linear alkyl side chains with thermal treatment in the UV–visible profile [6,16,32]. The additional peak at 434.8 nm was suggested to originate from an anti-coplanar structure (2_1 helix) [6,16,32]. Thus, it is reasonable to consider that although a similar thermally driven order–disorder conformational transition also occurred for **3** in THF upon cooling, the highly ordered motif is not a chiral helix, but an

Table 2
Characteristics of the PFs in the pristine and annealed thin films on quartz substrates

	Pristine thin film			Annealed thin film		
	λ_{max} (nm)	g_{CD} (nm)	$\lambda_{\text{eml}}(0-0)$ (nm)	P_{UV} (nm)	λ_{max} (nm)	g_{CD} (nm)
S1 ^a	378	-4.0×10^{-4} (356)	419.0	0.001 (375)	383	-0.18 (412)
S2	384	-1.6×10^{-4} (356)	421.0	0.004 (395)	383	-0.13 (430)
R2	384	$+1.3 \times 10^{-4}$ (356)	422.0	0.005 (395)	384	$+0.11$ (430)
3	386		426.5	0.006 (395)	395 ^b	

^a Run 2 sample of **S1**.

^b With a shoulder around 422 nm.

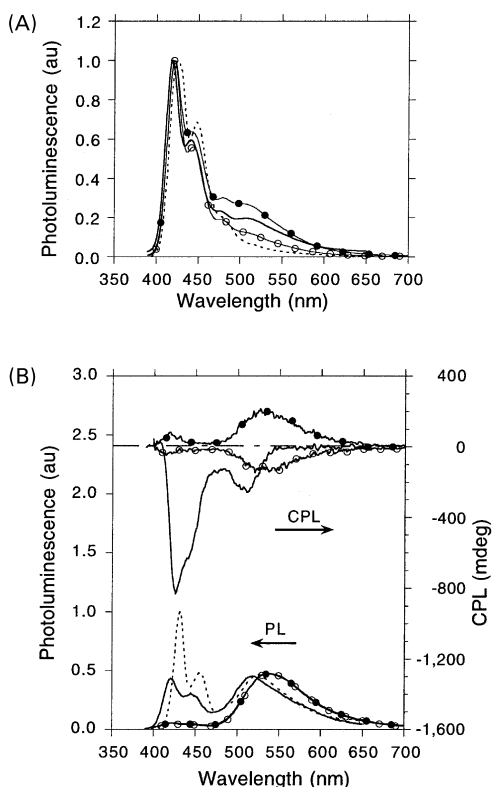


Fig. 4. CPL and PL spectra (excited at λ_{\max} s in the corresponding UV–visible spectra) of the PFs (thick solid line for **S1**; thin solid line with open circles for **S2**; thin solid line with filled circles for **R2**; dotted line for **3**) in the spin-coated pristine thin films (A) and the annealed thin films (B). Run 2 sample of **S1** was used.

anti-coplanar structure (2_1 helix) with the longest conjugation length having the lowest excitation energy.

3.1.2. Viscosity

A viscometric study is useful for obtaining information on the global conformational property of a polymer in an isotropic solution. We obtained the intrinsic viscosity, $[\eta]$, as a function of molecular weight, M , of each PF in THF at +30 °C. The viscosity index, α , tells us the degree of chain coiling of PF in THF at +30 °C from the Mark–Houwink–Sakurada plot, $[\eta] = \kappa \cdot M^\alpha$. A relatively high value of α such as 0.97 for **3**, 0.96 for **R2**, 0.98 for **S2**, and 1.07 for **S1** indicates that the PF backbone adopts a stiff conformation even in THF at +30 °C. The slightly larger value of α for **S1** suggests a fairly stiff PF backbone, probably responsible for the positive-sign CD signal in THF at +50 °C.

3.2. Solid-state properties

3.2.1. CD/UV–visible spectra

Fig. 3A compares the CD and UV–visible spectra of the PFs in pristine thin films. The characteristics are summarized in Table 2. The thin solid films, prepared by spin-coating from ~ 0.02 M THF solutions on quartz substrates, were transparent and showed extremely low linear dichroic

ratios, indicating that almost no ordered alignment of the PF backbones existed in the films. The CD spectrum of **S1** shows a bisignate CD signal with a positive-sign CD band at 399 nm and a negative-sign CD band at 356 nm in the region of the π – π^* transition of the PF backbone ($\lambda_{\max} = 378$ nm), probably due to the aggregates formed in the film. The dissymmetry factors in absorption, g_{CDs} , (which is defined as $g_{\text{CD}} = 2(\epsilon_{\text{L}} - \epsilon_{\text{R}})/(\epsilon_{\text{L}} + \epsilon_{\text{R}})$, where ϵ_{L} and ϵ_{R} denote the extinction coefficients for left and right circularly polarized light, respectively) were evaluated to be $+8.1 \times 10^{-4}$ at 399 nm and -4.0×10^{-4} at 356 nm. The CD spectrum of **S2** shows a similar bisignate CD signal, corresponding to the UV–visible spectrum exhibiting a redshift of 6 nm ($\lambda_{\max} = 384$ nm) in the absorption peak. The values of g_{CD} were ca. $+2.6 \times 10^{-4}$ at 399 nm and -1.6×10^{-4} at 356 nm, a factor of one-third of the absolute values of those of **S1**. **R2** showed an almost mirror-image CD spectrum of **S2** with g_{CD} of -2.5×10^{-4} at 399 nm and $+1.3 \times 10^{-4}$ at 356 nm. Furthermore, the UV–visible spectral profile of **3** in the pristine thin film ($\lambda_{\max} = 386$ nm) is similar to that of **S2** or **R2**.

The pristine thin films were annealed at 200 °C for 3 h in vacuo, and subsequently cooled slowly (~ 2 °C/h) to room temperature. The annealed thin films showed very low degrees of linear polarization in absorption, p_{UV} , as defined by $p_{\text{UV}} = 2(I_{\parallel} - I_{\perp})/(I_{\parallel} + I_{\perp})$, with I_{\parallel} and I_{\perp} the absorbance in two orthogonal polarization directions. As shown in Table 2, the values of p_{UV} are small, $\sim 10^{-3}$, and decrease in the order of **3**, **R2**, **S2**, and **S1**.

Fig. 3B compares the CD and UV–visible spectra of the PFs in the annealed thin films. The values of g_{CDs} are summarized in Table 2. As is evident, the annealing process led to dramatic changes in the CD and UV–visible spectra. The CD spectrum of **S1** in the annealed thin film exhibits an intense bisignate CD signal with a negative-sign CD band at 412 nm ($g_{\text{CD}} = -0.18$) and a positive-sign CD band at 385 nm ($g_{\text{CD}} = +0.06$), in association with the UV–visible spectrum showing a redshift of 5 nm ($\lambda_{\max} = 383$ nm) in the absorption peak and a significant broadening. The signs of the corresponding CD bands dramatically reversed, and the values of g_{CD} increased by about 200 times. The CD spectrum of **S2** in the annealed thin film shows three CD extrema at 430 nm ($g_{\text{CD}} = -0.13$), 398 nm ($g_{\text{CD}} = +0.15$) and 344 nm ($g_{\text{CD}} = -0.06$). The corresponding UV–visible spectrum shows broadening in the absorption band, but nearly no redshift in the absorption peak. An almost mirror-image CD spectrum of **S2** was obtained for **R2** in the annealed thin film, showing g_{CDs} of +0.11 at 430 nm, -0.11 at 398 nm and +0.03 at 344 nm. The facts of the very small values of p_{UV} and the mirror–image relationship between the CD spectra of **S2** and **R2** suggest that the CD signals are not due to some artifacts. In the case of **3**, the annealing process led to a redshift of 9 nm in the absorption peak ($\lambda_{\max} = 395$ nm) and especially, a newly appearing shoulder band around 422 nm. This indicates that the annealing process induced the planarization of the **3**

backbones and the formation of anti-coplanar structures in the annealed thin film [6,16]. The above conclusion that the CD signals of the optically active PFs in the annealed thin films are not due to some artifacts was further confirmed, because the alignment of **3** backbones in the annealed thin film gave rise to a negligible weak artificial signal with a g_{CD} of $+1.5 \times 10^{-4}$ at 395 nm.

3.2.2. CPL/PL spectra

Fig. 4A compares the PL spectra of the PFs in the pristine thin films. The wavelengths of the emitting bands due to the first (0–0) transitions decrease in the order of 426.5 nm for **3**, 422.0 nm for **R2**, 421.0 nm for **S2**, and 419.0 nm for **S1**, indicating that, with the stereocenters in the alkyl side chains closer to the PF backbones, the emitting motifs in the corresponding PF backbones have shorter conjugation lengths with higher photoexcited energies. This phenomenon is in agreement with the observations in the UV–visible spectra of the PFs in THF solutions and the pristine thin films (Figs. 1 and 3A).

Fig. 4B compares the CPL and PL spectra of the PFs in the annealed thin films. The characteristics of the g_{CPL} are given in Table 2. The CPL spectrum of **S1** exhibits an intense negative-sign emission band at 426 nm and a relatively weak negative-sign emission band at 511 nm, almost matching the emission band with a maximum at 420 nm and an intense featureless excimer emission band around 511 nm in the PL spectrum. The dissymmetry factors in emission, g_{CPLS} , (which is defined as $g_{CPL} = 2(I_L - I_R)/(I_L + I_R)$, where I_L and I_R denote the emission intensities for left and right circularly polarized light, respectively), were evaluated to be -0.07 at 426 nm and -0.02 at 511 nm. However, **S2** in the annealed thin film showed a relatively intense negative-sign band around 538 nm and a negligible weak negative-sign band at 426 nm in the CPL spectrum, corresponding to the intense featureless excimer band around 538 nm and the extremely weak band around 426 nm in the PL spectrum. Furthermore, **R2** in the annealed thin film showed an almost the same PL spectrum and an almost mirror-image CPL spectrum of **S2**. The values of g_{CPL} for **S2** and **R2** were evaluated to be -0.01 and $+0.01$ at 538 nm, respectively. This indicates that, in the annealed thin films of **S2** and **R2**, the emitting motifs are mainly of aggregates and/or excimers, probably due to the more highly ordered aggregated structures with shorter stacking distances between the neighboring PF backbones, compared to that of **S1**. The more highly ordered aggregated structures also led to the lower g_{CPLS} due to the quenching effect. Compared to the PL spectra of **S2** and **R2**, **3** in the annealed thin film, however, showed a PL spectrum exhibiting an intense emission band at 431 nm and a featureless excimer band at 525 nm. The reasons for the presence of the 431 nm emission band and the blueshift for the excimer emission band are not clear at present.

4. Conclusions

We prepared three optically active PFs, **S1**, **S2** and **R2**, featuring stereocenters at the β -, γ -positions in the alkyl side chains, together with an optically inactive **3** having linear alkyl side chains, and investigated the alkyl side-chain effects on their chiral/achiral optical properties in both solution and solid states. Among these PFs, **S1** showed the stiffest backbone structure and the most intense CD signals in THF solution at higher and lower temperatures. From the variable temperature CD and UV–visible spectra, it was suggested that all these PFs underwent similar thermally driven order–disorder conformational transitions. However, it was considered that the highly ordered conformations formed upon cooling showed less planar structures with the stereocenters became closer to the PF backbones: the backbone planarity decreased in the order of **3** (an anti-coplanar (2_1) structure), **S2/R2**, and **S1** (possibly a P -5₂ helix). In the pristine spin-coated thin films on quartz substrates, as the stereocenters closer to the PF backbones, the corresponding PFs gave more intense bisignate CD signals and blueshifts in the PL peaks. Randomly distributed orientations of the highly ordered aggregates of the planarized PF backbones in the annealed thin films were suggested by the film transparency and very low degrees of linear polarization in absorption. The optically active PFs in the annealed thin films gave high dissymmetry factors in absorption, g_{CDS} , of -0.18 at 412 nm for **S1**, and $+0.15$ and -0.11 at 398 nm for **S2** and **R2**, respectively. PF **S1** in the annealed thin film emitted an intense negative-sign CPL at 426 nm ($g_{CPL} = -0.07$) together with a relatively weak negative-sign excimer emission at 511 nm ($g_{CPL} = -0.02$). However, **S2** and **R2** emitted mainly a weak negative-sign and a positive-sign excimer emissions at 538 nm (g_{CPL} of -0.01 for **S2** and $+0.01$ for **R2**), respectively.

Acknowledgements

We greatly thank Prof. Julian R. Koe at International Christian University for kindly providing and instructing us on the LD measurements.

References

- [1] Neher D. *Macromol Rapid Commun* 2001;22:1365.
- [2] Leclerc M. *J Polym Sci, Part A: Polym Chem* 2001;39:2867.
- [3] Fukuda M, Sawada K, Yoshino K. *J Polym Sci, Part A: Polym Chem* 1993;31:2465.
- [4] Teetsov J, Fox MA. *J Mater Chem* 1999;9:2117.
- [5] Grell M, Bradley DDC, Inbasekaran M, Woo EP. *Adv Mater* 1997;9:798.
- [6] Grell M, Bradley DDC, Ungar G, Hill J, Whitehead KS. *Macromolecules* 1999;32:5810.
- [7] Grozema FC, Savenije TJ, Vermeulen MJW, Siebbeles LDA,

- Warman JM, Meisel A, Neher D, Nothofer HG, Scherf U. *Adv Mater* 2001;13:1627.
- [8] Cadby AJ, Lane PA, Mellor H, Martin SJ, Grell M, Giebeler C, Bradley DDC, Wohlgenannt M, An C, Vardeny ZV. *Phys Rev B* 2000;62:15604.
- [9] Shkunov MN, Österbacka R, Fujii A, Yoshino K, Vardeny ZV. *Appl Phys Lett* 1999;74:1648.
- [10] Redecker M, Bradley DDC, Inbasekaran M, Woo EP. *Appl Phys Lett* 1998;73:1565.
- [11] Janietz S, Bradley DDC, Grell M, Giebeler C, Inbasekaran M, Woo EP. *Appl Phys Lett* 1998;73:2453.
- [12] Grice AW, Bradley DDC, Bernius MT, Inbasekaran M, Wu WW, Woo EP. *Appl Phys Lett* 1998;73:629.
- [13] Redecker M, Bradley DDC, Inbasekaran M, Woo EP. *Appl Phys Lett* 1999;74:1400.
- [14] Herz LM, Phillips RT. *Phys Rev B* 2000;61:13691.
- [15] Weinfurter KH, Fujikawa H, Tokito S, Taga Y. *Appl Phys Lett* 2000;76:2502.
- [16] Grell M, Bradley DDC, Long X, Chamberlain T, Inbasekaran M, Woo EP, Soliman M. *Acta Polym* 1998;49:439.
- [17] Klaerner G, Miller RD. *Macromolecules* 1998;31:2007.
- [18] Pei QB, Yang Y. *J Am Chem Soc* 1996;118:7416.
- [19] Lieser G, Oda M, Miteva T, Meisel A, Nothofer HG, Scherf U, Neher D. *Macromolecules* 2000;33:4490.
- [20] Rothe C, Monkman A. *Phys Rev B* 2002;65:073201-1.
- [21] Bauer C, Urbasch G, Giessen H, Meisel A, Nothofer HG, Neher D, Scherf U, Mahrt RF. *Chem Phys Chem* 2000;142.
- [22] Fytas G, Nothofer HG, Scherf U, Vlassopoulos D, Meier G. *Macromolecules* 2002;35:481.
- [23] Sainova D, Zen A, Nothofer HG, Asawapirom U, Scherf U, Hagen R, Bieringer T, Kostromine S, Neher D. *Adv Funct Mater* 2002;12:49.
- [24] Marsitzky D, Vestberg R, Blainey P, Tang BT, Hawker CJ, Carter KR. *J Am Chem Soc* 2001;123:6965.
- [25] Marsitzky D, Vestberg R, Hawker CJ, Carter KR. *Polym Prepr (Am Chem Soc Polym Sci Div)* 2000;41(2):1344.
- [26] Setayesh S, Grimsdale AC, Weil T, Enkelmann V, Müllen K, Meghdadi F, List EJW, Leising G. *J Am Chem Soc* 2001;123:946.
- [27] Grimsdale AC, Herrmann A, Setayesh S, Weil T, Müllen K. *Polym Mater Sci Engng* 2001;84:6.
- [28] Tang HZ, Fujiki M, Zhang ZB, Torimitsu K, Motonaga M. *Chem Commun* 2001;2426.
- [29] Oda M, Nothofer HG, Lieser G, Scherf U, Meskers SCJ, Neher D. *Adv Mater* 2000;12:362.
- [30] Oda M, Meskers SCJ, Nothofer HG, Scherf U, Neher D. *Synth Meth* 2000;111/112:575.
- [31] Tang HZ, Fujiki M, Motonaga M, Torimitsu K. *Polym Prepr (Am Chem Soc Polym Sci Div)* 2001;42(1):440.
- [32] Tang HZ, Fujiki M, Sato T. *Macromolecules* 2002;35:6439.
- [33] Fujiki M. *Macromol Rapid Commun* 2001;22:669.
- [34] Fujiki M, Koe JR, Terao K, Sato T, Teramoto A, Watanabe J. *Polym J*. In preparation.
- [35] Fujiki M, Motonaga M, Tang HZ, Torimitsu K, Zhang ZB, Koe JR, Watanabe J, Terao K, Sato T, Teramoto A. *Chem Lett* 2001;1218.
- [36] Blok PML, Dekkers HPJM. *Appl Spectrosc* 1990;44:305.
- [37] Dekkers HPJM. Circularly polarized luminescence: a probe for chirality in the excited state. In: Berova N, Nakanishi K, Woody RW, editors. *Circular dichroism principles and applications*, 2nd ed. New York: Wiley/VCH; 2000. p. 199.